Available online at www.sciencedirect.com

SciVerse ScienceDirect

Ceramics International 39 (2013) 307–313

CERAMICS INTERNATIONAL

www.elsevier.com/locate/ceramint

Chemical stability and electrical properties of Nb doped $BaCe_{0.9}Y_{0.1}O_{3-\delta}$ as a high temperature proton conducting electrolyte for IT-SOFC

A. Radojković[a,*], M. Žunić[a,b], S.M. Savić[a], G. Branković[a], Z. Branković[a]

[a]Institute for Multidisciplinary Research, University of Belgrade, Kneza Višeslava 1a, 11030 Belgrade, Serbia
[b]Instituto de Química, UNESP—LIEC, CMDMC, Rua Prof. Francisco Degni, 55, CEP 14800-900, Araraquara, SP, Brazil

Received 18 May 2012; received in revised form 6 June 2012; accepted 7 June 2012
Available online 15 June 2012

Abstract

$BaCe_{0.9-x}Nb_xY_{0.1}O_{3-\delta}$ (where $x=0$, 0.01, 0.03 and 0.05) powders were synthesized by solid-state reaction to investigate the influence of Nb concentration on chemical stability and electrical properties of the sintered samples. The dense electrolyte pellets were formed from the powders after being uniaxially pressed and sintered at 1550 °C. The electrical conductivities determined by impedance measurements in temperature range of 550–750 °C in different atmospheres (dry argon and wet hydrogen) showed a decreasing trend with an increase of Nb content. For all samples higher conductivities were observed in the wet hydrogen than in dry argon atmosphere. The chemical stability was enhanced with increasing of Nb concentration. It was found that $BaCe_{0.87}Nb_{0.03}Y_{0.1}O_{3-\delta}$ is the optimal composition that satisfies the opposite demands for electrical conductivity and chemical stability, reaching 0.8×10^{-2} S cm^{-1} in wet hydrogen at 650 °C compared to 1.01×10^{-2} S cm^{-1} for undoped electrolyte.

Keywords: C. Ionic conductivity; D. Perovskites; E. Fuel cells

1. Introduction

Materials with perovskite structure based on barium cerate ($BaCeO_3$) have been widely investigated as electrolytes for intermediate-temperature solid oxide fuel cells (IT-SOFC). They expose proton conductivity when Ce^{4+} is substituted with small amounts of aliovalent cations such as Y^{3+}, In^{3+} and other rare earth cations (Gd^{3+}, Sm^{3+}, etc.) [1–6]. These cations cause the formation of point microstructure defects, i.e. oxygen ion vacancies (1) that further react with hydrogen, (2) or water vapor and (3) according to the following mechanism using Kröger–Vink notation [3,7,8]:

$$CeCe^{x}+1/2O_{O}^{x}+1/2M_2O_{3(s)}\rightarrow MCe'+1/2V_{O}^{\bullet\bullet}+CeO_{2(s)} \quad (1)$$

$$H_{2(g)}+V_{O}^{\bullet\bullet}+2O_{O}^{x}\leftrightarrow 2OH_{O}^{\bullet} \quad (2)$$

$$H_2O_{(g)}+V_{O}^{\bullet\bullet}+O_{O}^{x}\leftrightarrow 2OH_{O}^{\bullet} \quad (3)$$

The transport process of protons can be described by Grotthuss mechanism, where a relatively small activation energy is necessary (0.4–0.7 eV) for a proton to hop from one oxygen ion site to adjacent one. The reactions (2) and (3) were shown to be exothermal [9], which means that the proton conduction is dominant at lower temperatures, while at higher temperatures the reaction equilibrium is shifted towards the formation of oxygen vacancies, thus favouring a conducting mechanism that involves oxygen ions.

However, compared to oxygen-ion conductors, the protonic ones expose higher conductivities at lower temperatures, allowing SOFCs to be made of cheaper materials, which in addition to lower operating temperatures will reduce the overall costs of their usage. The another advantage of the proton conducting SOFCs is that water vapor, as the product of the electrochemical reaction, emanates at the cathode site, thus preventing dilution of the fuel fed at the anode site, which is the case in the oxide-ion conducting SOFCs [10,11].

*Corresponding author. Tel.: +381 11 2085037; fax: +381 11 2085038.
E-mail address: aleksandarrr@imsi.bg.ac.rs (A. Radojković).

0272-8842/$36.00
http://dx.doi.org/10.1016/j.ceramint.2012.06.026

Despite its high conductivity has been challenged by recent investigations [6], $BaCe_{0.9}Y_{0.1}O_{3-\delta}$ (BCY10) is recognized as one of the best perovskite-based proton conductors.

On the other hand, the main drawback of BCY10 is its chemical stability. The presence of CO_2 and water vapor at raised temperatures extensively deteriorate its microstructure, negatively affecting the electrical properties and durability of SOFCs [12,13]. Many investigations have been done on how to improve the chemical stability of barium cerates, all of which could be roughly divided into two main approaches. The first is to make solid solutions of barium cerates and more stable barium zirconates [14,15] and the second is co-doping B-sites with various cations such as Nb or Zr that would provide good stability [16–18]. Yet, it is normal to expect lower conductivities on account of chemical stability and other way round, which implies defining the optimal solution as a chemically stable system without significantly reduced conductivity.

It has been previously reported [18] that amounts of 0.03–0.12 mol% Nb^{5+} can secure satisfactory stability, but with solemn decline of electrical properties. The aim of this work is to investigate the influence of lower concentrations of Nb^{5+} (up to 0.05 mol%) on chemical stability and electrical properties of BCY10 and to determine the optimal concentration of Nb in BCY10 that will provide chemically stable microstructure with good electrical conductivity.

2. Experimental

2.1. Synthesis of the ceramic powders by solid-state reaction (SSR) method

$BaCe_{0.9-x}Nb_xY_{0.1}O_{3-\delta}$ (BCNY) powders (where $x=0$, 0.01, 0.03 and 0.05), denoted as BCY10, BCNY001, BCNY003 and BCNY005, were synthesized by the method of solid state reaction. Barium(II)-carbonate (Merck, 99%), cerium(IV)-oxide (Carlo Erba), yttrium(III)-oxide (Merck) and niobium(V)-oxide were homogenized with isopropyl-alcohol for 24 h in a planetary ball mill using tungsten carbide jar and balls. The mixture was dried at 50 °C for 2 h and ground in an agate mortar. Then the powders were fired at 1000 °C for 5 h to initiate the solid state reaction. Since the XRD patterns proved the existence of single BCNY phase, the powders were ground again, sieved through a 75 μm mesh, uniaxially pressed before sintering at 1550 °C for 5 h.

2.2. Characterization

The characterization of the powders was performed by differential scanning calorimetry-thermogravimetric (DSC-TGA) analysis (SDT Q600 V7.0 Build 84) and X-ray diffraction (XRD) analysis. The microstructure of the sintered pellets was also investigated by scanning electron microscopy (SEM) (TESCAN Vega TS5130MM) and XRD analysis.

Electrical characterization was performed on Pt/BCNY/Pt symmetrical cells within temperature range of 550–750 °C in wet H_2 (3 vol% H_2O) and in dry Ar atmosphere. This temperature range was chosen because it is the range of working temperatures for IT-SOFCs. The samples were prepared for electrical measurements by applying a thin Pt-paste layer on both sides of the pellets. The pellets with Pt-paste had been dried at 100 °C for 2 h before being treated for 30 min at 750 °C. Electrochemical impedance spectroscopy (EIS) was performed using a HIOKI 3532-50 LCR HiTESTER in a frequency range between 42 Hz and 1 MHz. The wet hydrogen atmosphere was provided by letting the gas through a gas washer filled with distilled water at the room temperature. In the other case, to secure dry argon medium the gas was passing through a gas trap filled with P_2O_5 prior to entering the aperture. In both cases the flow rate of the gases through the system was kept at 50 cm^3/min using a digital mass flow controller and meter (MKS PR 4000B-F).

2.3. Chemical stability

The sintered pellets were exposed to CO_2 atmosphere at 700 °C for 5 h by keeping the flow rate of CO_2 through the aperture at 400 cm^3/min. After being exposed the pellets were investigated by the XRD analysis in order to determine the changes in their microstructure.

3. Results and discussion

3.1. DSC-TGA analysis and X-ray diffraction patterns

In order to find out optimal processing conditions for synthesis of BCNY powders by the SSR method, it is suitable to start from the results of the DSC-TGA analysis. In Fig. 1 the DSC-TGA analysis of BCNY003 powder is shown. The first endothermic peak on the heat flow curve indicates the transformation from an orthorombic α-$BaCO_3$ phase to a trigonal, β-$BaCO_3$ phase at 811 °C

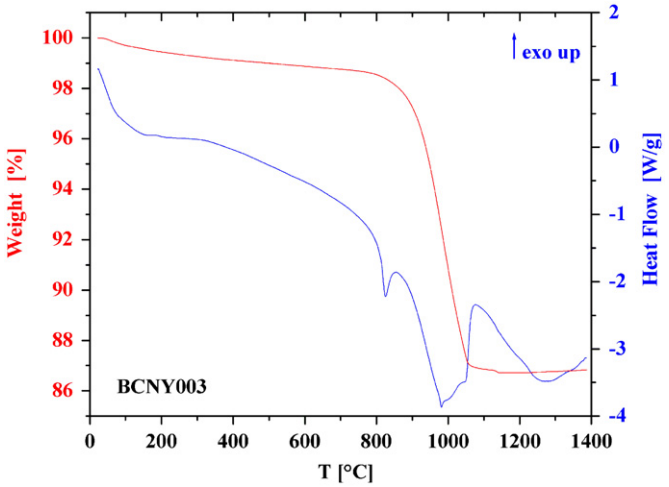

Fig. 1. DSC-TGA analysis of BCNY003 powder.

[19]. The next endothermic trend appears between 850 and 1050 °C, followed by a weight loss of approx. 10% on the weight loss curve that occurs due to the following reaction:

$$BaCO_{3(s)} + (0.9-x)CeO_{2(s)} + 0.05Y_2O_{3(s)} + (x/2)Nb_2O_{5(s)} \rightarrow BaCe_{0.9-x}Nb_xY_{0.1}O_{3-\delta(s)} + CO_{2(g)} \quad (4)$$

which is a modified version of the reaction reported elsewhere [20,21], taking into account the incorporation of dopants into the perovskite structure. All XRD spectra of the samples from the same batch calcined for 5 h in air at 1350, 1100 and 1000 °C show only the presence of BCNY phase, confirming that the formation of pure perovskite phase can be obtained even at 1000 °C. In Fig. 2 XRD pattern of BCNY003 powder calcined at 1000 °C for 5 h was shown demonstrating the presence of single orthorhombic phase. As it can be seen from Fig. 2 doping with Nb causes a slight shift of the reflection lines indicating a deformation of the crystal lattice of the undoped material. This can be explained by the incorporation of Nb^{5+} cations with smaller radii than Ce^{4+} and Y^{3+} (0.64 Å compared to 0.87 Å for Ce^{4+} and 0.90 Å for Y^{3+}) into BO_6 octahedra and causing their distortion [2,6,18].

3.2. Microstructure and phase purity of the sintered samples

Electrical properties of ceramic materials are strongly dependant on their microstructure. Microstructure features such as porosity and grain boundaries play important role in transport of charged species through material. Therefore, to enhance its conductivity it is necessary to form a dense microstucture, without or with minimal porosity. Fig. 3 shows SEM micrographs of the surface of the samples sintered at 1550 °C for 5 h. The resulting densities of the sintered samples reached 92–96% of the theoretic density for BCY10. Any specific influence of Nb concentration on the density value was not marked. The grain boundaries are flat in almost all volumes of the samples, indicating that the sintering process is finished.

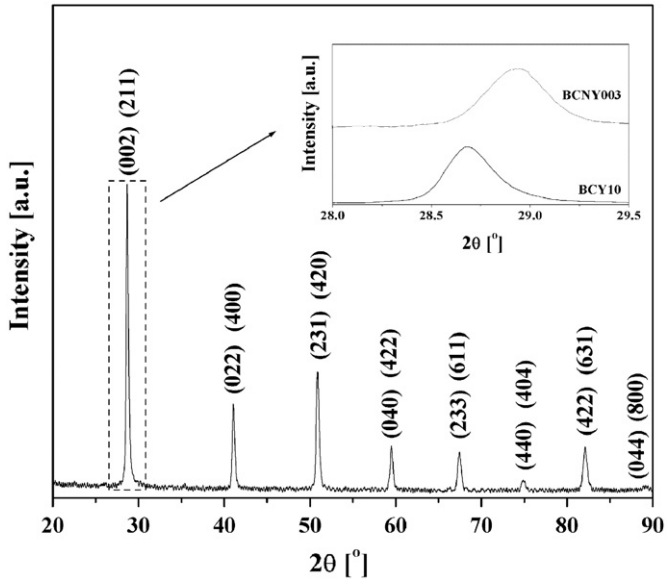

Fig. 2. XRD pattern of BCNY003 powder calcined at 1000 °C for 5 h. The reflection lines of undoped BCY10 (JCPDS card no.81-1386) are also shown as a reference.

The average grain size were 1.6 μm (BCY10), 1.5 μm (BCNY001), 1.2 μm (BCNY003) and 1.1 μm (BCNY005) which is similar to data found in literature [18,22,23]. It can be noticed from the SEM images that the average grain size decreases with the increase in dopant concentration. It means that the samples with higher dopant concentrations contain more grain boundaries per volume unit. If the grain boundaries in this case represent barriers to the transport of charged species, a decrease in electrical conductivities could be expected with an increase in dopant concentration. The larger the average grain size is, the lower the contribution of the grain boundaries is in the path of the charge carriers. Another characteristic of the BCY10 ceramics is a bimodal grain size distribution as can be clearly seen at the BCNY001 sample (Fig. 3b). Thus, the nature and concentration of dopants can influence sinterability, grain size pattern of sintered ceramics and consequently their electrical properties [4,6,15,18,22,23].

3.3. Electrical properties

As a result of good microstructural characteristics, the sintered electrolyte materials should have good electrical characteristics. Fig. 4 shows Nyquist plot of BCNY005 at 650 °C in the dry argon atmosphere. Experimental data were fitted using EIS Spectrum Analyzer Software and the equivalent circuit as a fitting model was composed of an inductor, L, resistors R_1, R_2, R_3 and constant phase elements, denoted as CPE_1 and CPE_2. In the frequency range shown in Fig. 4 the EIS spectrum consists of two overlapping depressed semicircles. The first one, around 20 kHz, is related to grain boundary since the calculated capacitance of 9.6×10^{-10} F cm^{-1} is in order of magnitude typical for grain boundary capacitance [24,25]. It was calculated by using the following equation [23,26]:

$$C = R^{\frac{1-n}{n}}Q^{\frac{1}{n}} \quad (5)$$

where Q is a pre-exponential factor and n is an exponent of the CPE ($0 \leq n \leq 1$).

The capacitance of 1.3×10^{-6} F cm^{-1}, calculated for the second arc in a lower frequency region (around 2 kHz) refers to processes at electrolyte/electrode interface. Thus, at the temperature range 550–750 °C it was difficult to separate contributions of grain boundary and bulk resistivity to the total resistivity of all samples both in the dry argon and wet hydrogen atmosphere. Nevertheless, it was possible to determine the total conductivities which increased with temperature for each sample. Fig. 5 shows Arrhenius plots of the conductivity values of the BCNY samples, obtained from EIS measurements at different temperatures in the wet hydrogen medium.

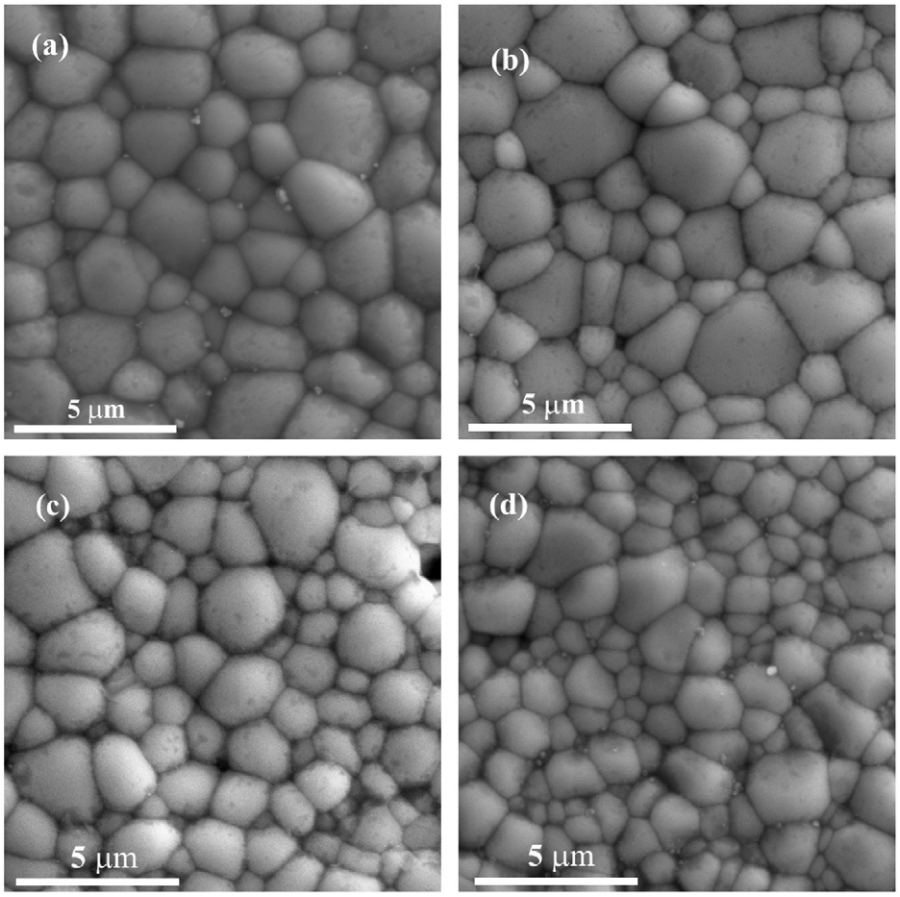

Fig. 3. SEM images of the surface of the sintered samples: (a) BCY10, (b) BCNY001, (c) BCNY003 and (d) BCNY005.

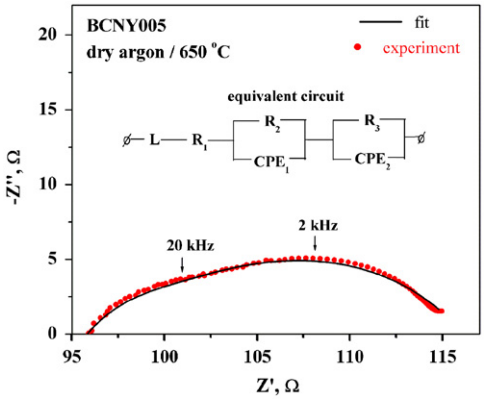

Fig. 4. Impedance spectra of BCNY005 sample in the dry argon atmosphere at 650 °C.

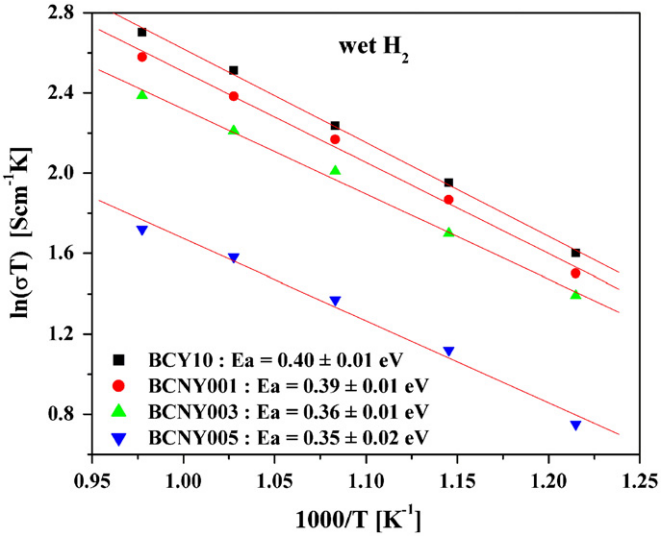

Fig. 5. Temperature dependence in the form of Arrhenius plots of the conductivities measured in the wet H_2 atmosphere.

Nb reduced the conductivitiy of BCY10 in the whole temperature range. The lowest conductivities, as it was expected, were measured for the sample with 5 mol% of Nb: 4.25×10^{-3} S cm^{-1} at 650 °C in the wet hydrogen medium compared to 1.01×10^{-2} S cm^{-1} for BCY10 at the same conditions. These results are in accordance with the results reported elsewhere [18] and the assumption stated in the previous section on how grain size and microstructure can influence the electrical properties. Besides, doping of BCY10 usually causes a certain lattice disorder which leads to decrease in conductivities as well [2,6,18]. Doping with 1 and 3 mol% of Nb slightly reduces the conductivities of BCY10, while introducing 5 mol% of Nb significantly decreases the conductivity in the wet hydrogen atmosphere. Co-doping of Nb and Y can be

described by following equations:

$$CeCe^{x} + 1/2O_{O}^{x} + 1/2\,Y_2O_{3(s)} \rightarrow Y_{Ce'} + 1/2V_{O}^{\bullet\bullet} + CeO_{2(s)} \quad (6)$$

$$CeCe^{x} + 1/2V_{O}^{\bullet\bullet} + 1/2Nb_2O_{5(s)} \rightarrow Nb_{Ce}^{\bullet} + 1/2O_{O}^{x} + CeO_{2(s)} \quad (7)$$

This means that a positive charge created by Nb^{5+} occupying Ce^{4+} sites in the octahedra of the oxygen ion sublattice will be compensated by a negative charge as a consequence of simultaneous replacement of Ce^{4+} with Y^{3+}. Since the maximal concentration of Nb (5 mol%) is lower than that of Y (10 mol%), the excess amount of yttrium is responsible for creation of oxygen vacancies according to Eqs. (1) and (6). This decrease in concentration of oxygen vacancies with Nb concentration will reduce the conductivity due to the mechanisms described by Eqs. (2), (3) and (7), which is in agreement with the experimental data (Fig. 5 and Fig. 6a). The activation energies obtained from Arrhenius plots for bulk conductivities in the wet hydrogen atmosphere are ~0.4 eV and are similar for all samples in the temperature range of 550–750 °C.

On the other hand, in the dry argon atmosphere, where there is no source of protons, the measured conductivities are lower for each concentration of Nb at given temperature than in the wet hydrogen atmosphere (Fig. 6a and b).

This is also reasonable due to absence of protons in the expression for the total conductivity that equals the sum of the conductivities of existing charge carriers:

$$\sigma_{\text{total}} = \sum_i \sigma_i = \sum_i D_i c_i \mu_i \quad (8)$$

where σ_i represents conductivity, D_i is the diffusion coefficient, c_i is the concentration and μ_i is the mobility of the charge carriers. Apart from oxygen vacancies, other point defects, like electron holes, can arise at higher temperatures in an atmosphere with high partial pressure of oxygen, i.e. during sintering in air [15,20,27,28]:

$$V_{O}^{\bullet\bullet} + 1/2O_{2(g)} \leftrightarrow O_{O}^{x} + 2h^{\bullet} \quad (9)$$

In wet atmospheres the water uptake may also occur by positively charged electron holes [27] according to:

$$H_2O_{(g)} + 2O_{O}^{x} + 2h^{\bullet} \rightarrow 2OH_{O}^{\bullet} + 1/2O_{2(g)} (\sigma_h^{\bullet} \sim p(O_2)^{1/4}) \quad (10)$$

where electron holes conductivity is decreased on account of proton conductivity.

Bearing this in mind it is assumed that in a wet hydrogen medium proton conductivity dominates at lower temperature, while oxygen ions conductivity is enhanced at higher temperatures, i.e. over 650 °C according to Table 1, provided that electron holes conductivity is negligible due to Eq. (10) and at low partial pressure of oxygen. In a dry argon atmosphere the electron holes conductivity is dominant at lower temperatures, while the oxygen ions conductivity contribution is expected at higher temperatures. According to Table 1, the highest relative differences between conductivities in the wet hydrogen and dry argon atmosphere reach maximal values at 650 °C for all samples referring to the highest contribution of proton conductivity at this temperature. These differences increase with Nb concentration and the highest values are observed for the

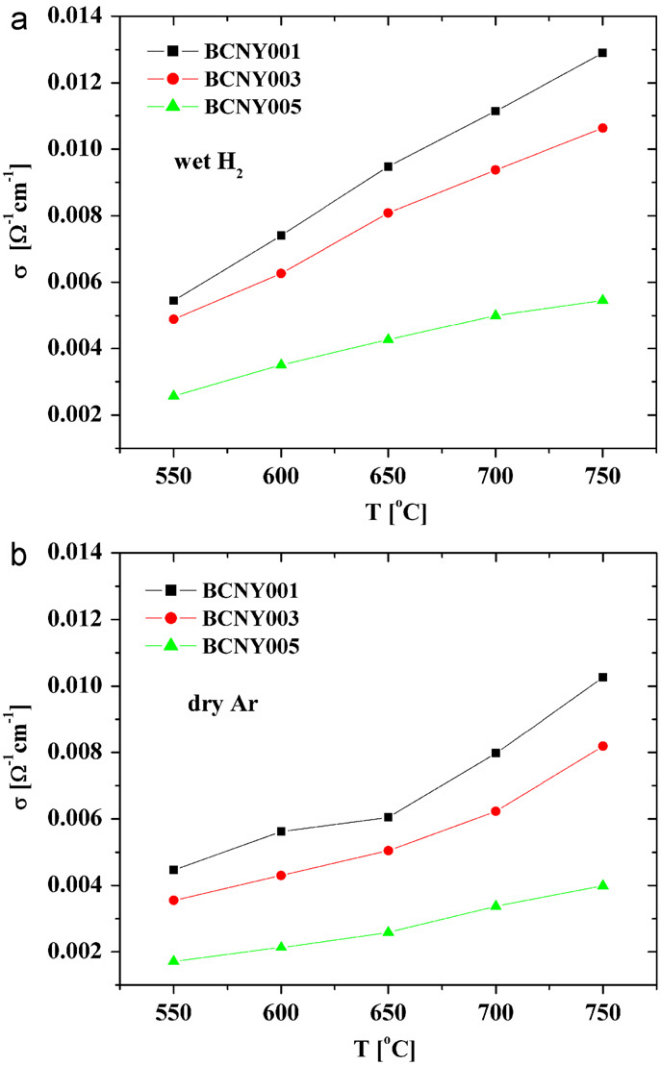

Fig. 6. Total conductivities of BCNY001, BCNY003 and BCNY005 samples at temperature range 550–750 °C: (a) in wet H_2 and (b) in dry Ar.

Table 1
Relative difference between total conductivities in the wet hydrogen and dry argon atmosphere.

Conductivity (S cm^{-1})			
T (°C)	[σ(in H_2/H_2O) − σ(in Ar)]/σ(in H_2/H_2O) (%)		
	BCNY001	BCNY003	BCNY005
750	20.2	22.8	26.9
700	28.8	33.5	32.4
650	36.2	37.5	39.3
600	24.2	31.4	39.3
550	18.0	27.4	33.5

BCNY005 sample. It is found [9,29] that molar enthalpy of the exothermal reaction described by Eq. (3) depends on the electronegativity of dopants and may be calculated from the following expression:

$$\Delta H_3(kJ/mol) = -173(9) + 370(42)\Delta X_{B-A} \quad (11)$$

where ΔX_{B-A} is the difference in electronegativity between A-site and B-site constituents. As Nb has higher electronegativity (1,6) than Y (1,22) or Ce (1,12), the hydration of oxygen vacancies will become less exothermal with an increase in Nb concentration according to Eq. (9), thus allowing higher proton concentrations even at temperatures above 650 °C. At lower temperatures, and considering Eq. (9), the concentration of electron holes is expected to decrease with Nb amount as the concentration of vacancies is reduced according to Eqs. (1) and (7). As a result, Nb appears to promote proton conducting in respect to other conducting mechanisms although the overall conductivity decreases with its content as observed at temperatures between 550 and 750 °C.

3.4. Chemical stability of BCNY

Good chemical stability of electrolyte materials is very important for their IT-SOFC application, especially when SOFCs operate with carbon containing fuels. It is known that the main drawback of using BCY10 as an electrolyte for SOFC is its microstructure deterioration in the presence of CO_2 at higher temperatures [4,13–18,25]. Fig. 7 shows XRD spectra of the sintered samples after exposure to 100% CO_2 atmosphere at 700 °C for 5 h. The presence of BCNY, $BaCO_3$ and CeO_2 phases were indicated and hence it was easy to assume the reaction mechanism due to which BCY10 dissolves when being exposed to CO_2:

$$BaCeO_{3(s)} + CO_{2(g)} \rightarrow BaCO_{3(s)} + CeO_{2(s)} \quad (12)$$

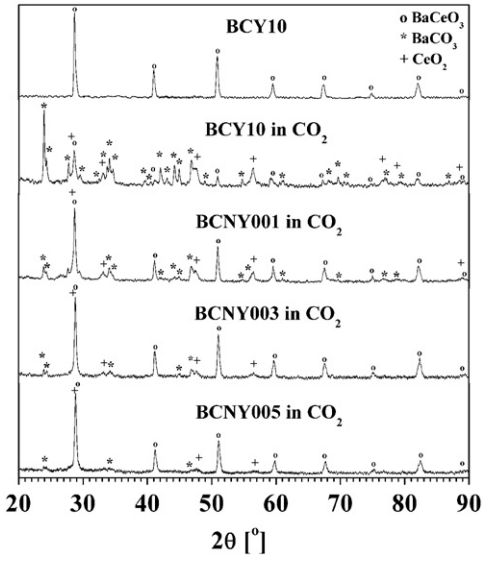

Fig. 7. XRD spectra of the undoped BCY10 and Nb-doped ceramics after being exposed to 100% CO_2 atmosphere at 700 °C for 5 h.

This reaction has been proven to be inhibited by doping BCY10 with oxides such as Nb_2O_5, whwereas a relatively high electronegativity of Nb is responsible for raised acidity of the crystal lattice [18]. It is clear from Fig. 7 that the presence of Nb stabilizes BCY10 in CO_2 atmosphere at raised temperatures as the peaks of the secondary phases are less expressed with Nb content. A significant improvement of stability is noticed even for the BCNY003 sample taking in consideration that the testing conditions for stability (100% CO_2 atmosphere at 700 °C for 5 h) were too extreme compared to those that usually develop during performance of SOFC applications based on hydrocarbon fuels [10,18]. Further increase in Nb concentration would probably enhance the stability, but at the same time the conductivities less than 10^{-3} S cm^{-1} will not secure efficient IT-SOFC application.

4. Conclusion

The electrical properties Nb-doped BCY10 ceramics were investigated in the wet hydrogen and dry argon atmosphere at temperatures between 550 and 750 °C as well as the stability after their exposure to 100% CO_2 at 700 °C for 5 h. The total conductivities decreased with Nb concentration both in the wet hydrogen and dry argon medium, while the highest conductivities were obtained in the wet hydrogen atmosphere. The average grain size was the smallest and the conductivities both in the wet hydrogen and dry argon atmosphere were lowest for the BCNY005 sample. The total conductivities increased with temperature for all samples in both media. Although Nb content negatively influence the electrical properties, it may favor proton conducting against other conducting mechanisms at temperatures above 650 °C since the enthalpy for vacancy hydration becomes less exothermal with an increase in Nb content. The highest contribution of the proton conducting to the overall conductivity is observed at 650 °C for all samples. When it comes to stability in CO_2, the presence of Nb prevents the degradation of BCY10 ceramics and the BCNY003 sample is considered to achieve significant stability. Its conductivity at 650 °C in the wet hydrogen medium (0.8×10^{-2} S cm^{-1}) still remains competitive since it is slightly lower than that for undoped BCY10 (1.0×10^{-2} S cm^{-1} in the same conditions).

Acknowledgments

The authors acknowledge that this work was supported by the Ministry of Education and Science of the Republic of Serbia (Project no. III45007) and Fundação de Amparo à Pesquisa do Estado de Saõ Paulo-FAPESP (Project no. 2010/20574-3). The authors also appreciate the valuable help of Dejan Poleti, Đorđe Janaćković and Jelena Miladinović, professors at the Faculty of Technology and Metallurgy, University of Belgrade.

References

[1] N. Bonanos, B. Ellis, M.N. Mahmood, Construction and operation of fuel cells based on the solid electrolyte $BaCeO_3$:Gd, Solid State Ionics 44 (1991) 305.

[2] H. Iwahara, T. Yajima, H. Ushida, Effect of ionic radii of dopants on mixed ionic conduction ($H^+ + O^{2-}$) in $BaCeO_3$-based electrolytes, Solid State Ionics 70/71 (1994) 267.

[3] D. Shima, S.M. Haile, The influence of cation non-stoichiometry on the properties of undoped and gadolinia-doped barium cerate, Soild State Ionics 97 (1997) 443.

[4] L. Bi, S. Zhang, L. Zhang, Z. Tao, H. Wang, W. Liu, Indium as an ideal functional dopant for a proton-conducting solid oxide fuel cell, International Journal of Hydrogen Energy 34 (2009) 2421.

[5] F. Zhao, F. Chen, Performance of solid oxide fuel cells based on proton conducting $BaCe_{0.7}In_{0.3-x}Y_xO_{3-\delta}$ electrolyte, International Journal of Hydrogen Energy 35 (2010) 11194.

[6] M. Amsif, D. Marrero-Lopez, J.C. Ruiz-Morales, S.N. Savvin, M. Gabás, P. Nunez, Influence of rare-earth doping on the microstructure and conductivity of $BaCe_{0.9}Ln_{0.1}O_{3-\delta}$ proton conductors, Journal of Power Sources 196 (2011) 3461.

[7] K.D. Kreuer, On the development of proton conducting materials for technological applications, Solid State Ionics 97 (1997) 1.

[8] A. Kruth, J.T.S. Irvine, Water incorporation studies on doped barium cerate perovskites, Solid State Ionics 162 (163) (2003) 83.

[9] T. Norby, Solid-state protonic conductors: principles, properties, progress and prospects, Solid State Ionics 125 (1999) 1.

[10] S.M. Haile, Fuel cell materials and components, Acta Materialia 51 (2003) 5981.

[11] H. Iwahara, Y. Asakura, K. Katahira, M. Tanaka, Prospect of hydrogen technology using proton-conducting ceramics, Solid State Ionics 168 (2004) 299.

[12] M.J. Scholten, J. Schoonman, J.C. van Miltenburg, H.A.J. Oonk, Synthesis of strontium and barium cerate and their reaction with carbon dioxide, Solid State Ionics 61 (1993) 83.

[13] N. Bonanos, K.S. Knight, B. Ellis, Perovskite solid electrolytes: structure, transport properties and fuel cell applications, Solid State Ionics 79 (1995) 161.

[14] J. Lv, L. Wang, D. Lei, H. Guo, R.V. Kumar, Sintering, chemical stability and electrical conductivity of the perovskite proton conductors BaCe0.45Zr0.45M0.1O3-δ (M=In, Y, Gd, Sm), Journal of Alloys and Compounds 467 (2009) 376.

[15] S. Ricote, N. Bonanos, Enhanced sintering and conductivity study of cobalt or nickel doped solid solution of barium cerate and zirconate, Solid State Ionics 181 (2010) 694.

[16] C. Zuo, T.H. Lee, S.E. Dorris, U. Balachandran, M. Liu, Composite Ni–$Ba(Zr_{0.1}Ce_{0.7}Y_{0.2})O_3$ membrane for hydrogen separation, Journal of Power Sources 159 (2006) 1291.

[17] K. Katahira, Y. Kohchi, T. Shimura, H. Iwahara, Protonic conduction in Zr-substituted $BaCeO_3$, Solid State Ionics 138 (2000) 91.

[18] E. Di Bartolomeo, A. D'Epifanio, C. Pugnalini, F. Giannici, A. Longo, A. Martorana, S. Licoccia, Structural analysis, phase stability and electrochemical characterization of Nb doped $BaCe_{0.9}Y_{0.1}O_{3-x}$ electrolite for IT-SOFCs, Journal of Power Sources 199 (2012) 201.

[19] S.M. Antao, I. Hassan, $BaCO_3$: high-temperature crystal structures and the $Pmcn \rightarrow R3m$ phase transition at 811 °C, Physics and Chemistry of Minerals 34 (2007) 573.

[20] K. Künstler, H.-J. Lang, A. Maiwald, G. Tomandl, Synthesis, structure and electrochemical properties of In-doped $BaCeO_3$, Solid State Ionics 107 (1998) 221.

[21] N.I. Matskevich, Enthalpy of formation of $BaCe_{0.9}In_{0.1}O_{3-\delta}$, Journal of Thermal Analysis and Calorimetry 90 (2007) 955.

[22] X.-T. Su, Q.-Z. Yan, X.-H. Ma, W.-F. Zhang, C.-C. Ge, Effect of co-dopant addition on the properties of yttrium and neodymium doped barium cerate electrolyte, Solid State Ionics 177 (2006) 1041.

[23] M. Khandelwal, A. Venkatasubramanian, T.R.S. Prasanna, P. Gopalan, Correlation between microstructure and electrical conductivity in composite electrolytes containing Gd-doped ceria and Gd-doped barium cerate, Journal of the European Ceramic Society 31 (2011) 559.

[24] T.S. Bjørheim, A. Kuwabara, I. Ahmed, R. Haugsrud, S. Stølen, T. Norby, A combined conductivity and DFT study of protons in $PbZrO_3$ and alkaline zirconate perovskites, Solid State Ionics 181 (2010) 130.

[25] L. Bi, E. Fabbri, Z. Sun, E. Traversa, Sinteractivity, proton conductivity and chemical stability of $BaZr_{0.7}In_{0.3}O_{3-\delta}$ for solid oxide fuel cells (SOFCs), Solid State Ionics 196 (2011) 59.

[26] B. Hirschorn, M.E. Orazem, B. Tribollet, V. Vivier, I. Frateur, M. Musiani, Determination of effective capacitance and film thickness from constant-phase-element parameters, Electrochimica Acta 55 (2010) 6218.

[27] H. Uchida, N. Maeda, H. Iwahara, Relation between proton and hole conduction in $SrCeO_3$-based solid electrolytes under water-containing atmospheres at high temperatures, Solid State Ionics 11 (1983) 117.

[28] H. Iwahara, Ionic conduction in perovskite-type compounds in: T. Ishihara (Ed.), Perovskite Oxide for Solid Oxide Fuel Cells, Springer, Dordrecht, Heidelberg, London, New York, 2009, pp. 45–62.

[29] T. Norby, Proton Conductivity in Perovskite Oxides, in: T. Ishihara (Ed.), Perovskite Oxide for Solid Oxide Fuel Cells, Springer, Dordrecht, Heidelberg, London, New York, 2009, pp. 217–238.